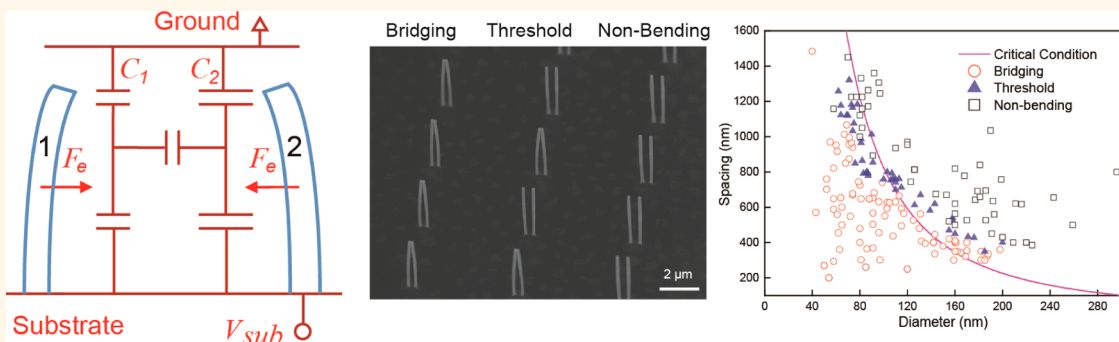


# Self-Bridging of Vertical Silicon Nanowires and a Universal Capacitive Force Model for Spontaneous Attraction in Nanostructures

Zhelin Sun,<sup>†</sup> Deli Wang,<sup>\*,†,‡,§</sup> and Jie Xiang<sup>\*,†,‡</sup>

<sup>†</sup>Department of Electrical and Computer Engineering, <sup>‡</sup>Materials Science and Engineering Program, and <sup>§</sup>Qualcomm Institute, University of California—San Diego, La Jolla, California 92093, United States

## ABSTRACT



Spontaneous attractions between free-standing nanostructures have often caused adhesion or stiction that affects a wide range of nanoscale devices, particularly nano/microelectromechanical systems. Previous understandings of the attraction mechanisms have included capillary force, van der Waals/Casimir forces, and surface polar charges. However, none of these mechanisms universally applies to simple semiconductor structures such as silicon nanowire arrays that often exhibit bunching or adhesions. Here we propose a simple capacitive force model to quantitatively study the universal spontaneous attraction that often causes stiction among semiconductor or metallic nanostructures such as vertical nanowire arrays with inevitably nonuniform size variations due to fabrication. When nanostructures are uniform in size, they share the same substrate potential. The presence of slight size differences will break the symmetry in the capacitive network formed between the nanowires, substrate, and their environment, giving rise to electrostatic attraction forces due to the relative potential difference between neighboring wires. Our model is experimentally verified using arrays of vertical silicon nanowire pairs with varied spacing, diameter, and size differences. Threshold nanowire spacing, diameter, or size difference between the nearest neighbors has been identified beyond which the nanowires start to exhibit spontaneous attraction that leads to bridging when electrostatic forces overcome elastic restoration forces. This work illustrates a universal understanding of spontaneous attraction that will impact the design, fabrication, and reliable operation of nanoscale devices and systems.

**KEYWORDS:** spontaneous attraction · bending · bridging · capacitive force · silicon nanowire · nanostructure fabrication · stiction

Spontaneous attraction, also known as spontaneous adhesion or stiction,<sup>1</sup> is a common but sometimes overlooked phenomenon among various nanostructures such as nanowires,<sup>2–8</sup> carbon nanotubes (CNTs),<sup>9</sup> graphene,<sup>10</sup> and nano/microelectromechanical systems (NEMS/MEMS).<sup>1,11–14</sup> In fact, the bending, collapsing, or stiction induced during device fabrication or operation often leads to unreliability such as poor

device performance and even failure. For instance, irreversible stiction is considered to be a major failure mode in NEMS/MEMS,<sup>14–16</sup> and the distortion of geometrical symmetry affects electron transportation properties or optical absorption in ordered nanowire arrays.<sup>17,18</sup>

Understanding the mechanism of spontaneous attraction on a quantitative level is critical for the fabrication of nanostructures

\* Address correspondence to d.w.wang@ieee.org, xiang@ece.ucsd.edu.

Received for review July 17, 2014 and accepted October 19, 2014.

Published online October 19, 2014  
10.1021/nn503924s

© 2014 American Chemical Society

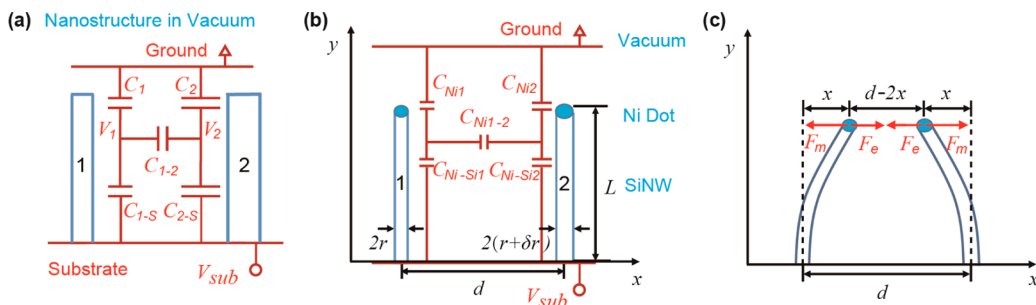


**Figure 1.** Capacitance force model. (a) Generic circuit diagram between semiconductor nanostructures in vacuum.  $C_1$  and  $C_2$  are self-capacitances;  $C_{1-s}$  and  $C_{2-s}$  are the capacitances between the nanostructures and substrate.  $C_{1-2}$  is the interactive capacitance between nanostructures;  $V_1$  and  $V_2$  are the potentials on the nanostructures. (b) Capacitance force model for a pair of vertical nanowires with spacing  $d$ , radius  $r$ , and length  $L$ .  $V_{sub}$  is the substrate voltage from surface charges, and ground is defined at a far away location from the sample, typically sample holders, instrument chambers, etc.  $C_{Ni}$ ,  $C_{Ni-Si1}$ , and  $C_{Ni1-2}$  are the capacitances on the SiNW with Ni dots on top.  $\delta r$  is the radius difference between the two nanowires. (c) Force diagram between a pair of nanowires.  $F_e$  is the attractive capacitive force, and  $F_m$  is the repulsive elastic force.  $x$  is the displacement of one of the nanowires.

and nanodevices. Explanations have included dispersion forces (van der Waals/Casimir forces),<sup>5,11–14,16,19–22</sup> capillary force,<sup>11,12,22–28</sup> and electrostatic force generated by surface polar charges.<sup>4</sup> These studies give a rather diverse picture, and many mechanisms either are not completely understood or only applicable in special circumstances. The van der Waals and Casimir attractive forces are very short-ranged, typically insignificant if the nanostructures are spaced beyond 50 nm apart<sup>29</sup> (see also Supporting Information Figures S1 and Figure S2), thus could not explain the long distance attraction among nanostructures.<sup>4,6,8</sup> Capillary force induced by solvent evaporation can explain bunching of nanostructures during drying but only applies in humid environments<sup>14</sup> or devices involving aqueous processing.<sup>23,26,28</sup> The polarized surface model<sup>30</sup> relies on the unique wurtzite structure of ZnO nanowires. More generally, self-attraction is also commonly observed on other materials such as silicon<sup>5</sup> and GaAs<sup>6</sup> that lack any of the above characteristics. Therefore, a more universal governing mechanism for spontaneous attraction remains to be explored.

In this article, we propose a universal capacitive force model based on the size variations and therefore variations in self-capacitance inherent to most fabricated nanostructures. In practice, although nanostructures are often surrounded by multiple structures of similar sizes, we would like to focus on two neighboring structures with the strongest interaction that will render them predominantly attracting each other and bending accordingly. This can mean, for example, two free-standing nanowires that are close to each other. We used high-aspect-ratio silicon nanowire (SiNW) arrays as an example system and performed systematic experiments to verify our model for spontaneous attraction. Spacing, diameter, and size difference are varied for these vertically aligned nanowire pairs and the experiments revealed the threshold dimensions for causing or avoiding spontaneous attraction, which agree very well with our model.

The mechanism behind the spontaneous bending and bridging of the NW pairs can be expressed with a simple capacitive force model, where the main source of attraction is considered to be the electrostatic interaction caused by capacitance difference between nanowires. Semiconductor and metallic nanostructures are typically anchored on a substrate to form a capacitive and resistive network between them (Figure 1a). The substrate carries a potential  $V_{sub}$  that originates from the natural charge distribution.<sup>31–34</sup> Its value and sign depend on the nature of the substrate material and the processing steps. We focus on steady-state electrostatic forces and ignore all transient behaviors. We can therefore ignore equivalent resistances here for simplicity because resistance values only affect transient behaviors, in other words, how fast or slow the network reaches the steady-state equilibrium solutions. Voltage reference (ground) is defined at very far away, which experimentally could represent the metal instrument chamber wall or a sample holder.

In Figure 1a, if the pair of nanostructures is symmetrical, with the same self-capacitances ( $C_1 = C_2$ ) and equal substrate capacitances ( $C_{1-s} = C_{2-s}$ ), the two nanowire surfaces would have the exact same potential and there will be zero electrostatic force between them. However, as no nanofabrication can yield atom-to-atom precision in size variability across neighboring structures, their capacitances are typically slightly different ( $C_1 \neq C_2$  and  $C_{1-s} \neq C_{2-s}$ ), leading to a potential difference between them ( $V_1 \neq V_2$ ), resulting in electric field lines emanating from the higher potential surface and terminating on the opposite surface. The resulting attractive electrostatic force will cause bending once it overcomes the mechanical restoration force of the nanostructures. In our experiments, we use reactive ion etched silicon nanowires as an example. The equivalent capacitive circuit for a pair of nanowires with nickel dots is shown in Figure 1b. The nickel dots served as masks during the reactive ion etching (RIE) process and were not removed from these SiNWs to

avoid any effect from capillary force during aqueous processing. The small size variation between nanowires after fabrication leads to a difference in their capacitances, including the self-capacitance of the nickel dot  $C_{\text{Ni}}$  and the Schottky junction capacitance  $C_{\text{Ni-Si}}$  between the nickel dot and the n-type SiNW. Consequently, there is a potential difference  $\delta V$  between nanowires, creating an attractive capacitive force that leads to spontaneous bending (Figure 1c). Note that the inclusion of a Ni dot at the tip is not necessary to generate attractive forces in generic nanostructures (Supporting Information, Figure S3).

Detailed calculation is given for a pair of nanowires with spacing  $d$ , radius  $r$ , radius difference  $\delta r$ , and length  $L$ . The nickel dot has a self-capacitance  $C_{\text{Ni}} = 4\pi\epsilon_0 r$ , where  $\epsilon_0 = 8.85 \times 10^{-12} \text{ F/m}$  is the vacuum permittivity. The Ni–Si junction capacitance can be readily calculated from a standard Schottky junction model:  $C_{\text{Ni-Si}} = C_0\pi r^2$ , where  $C_0 = \epsilon/X_d$  is the capacitance per unit area and  $X_d = (2\epsilon\phi/qN_d)^{1/2}$  is the width of depletion region. The n-SiNWs in our experiments have an average doping concentration  $N_d = 5 \times 10^{18} \text{ cm}^{-3}$ , a built-in potential  $\phi_b = 0.67 \text{ eV}$ , and a dielectric constant  $\epsilon = 11.68\epsilon_0$ .  $C_{\text{Ni-Ni}} = 4\pi\epsilon_0 r_1 r_2/d$  is a very small capacitance between Ni dots that only takes effect when nanowires are very close. In our experimental demonstration, since the substrate is electrically connected directly to the pair of nanowires by the same semiconducting Si material, the nanowire–substrate capacitances  $C_{1-s}$  and  $C_{2-s}$  in Figure 1a are replaced by the Schottky junction capacitance  $C_{\text{Ni-Si}}$ . The charges responsible for the differential potential between the two nanostructures are predominantly stored across  $C_{\text{Ni-Si}}$  in the Ni tips. All these capacitances are dependent on the nanowire radius  $r$ . When we assume there exists a radius variance  $\delta r$  between two nanowires, this size discrepancy will break the symmetry of capacitances and create a potential difference  $\delta V$  shown below:

$$\delta V = \frac{\beta \cdot C_{\text{Ni-Si1}} - C_{\text{Ni-Si2}}}{C_{\text{Ni1}} + C_{\text{Ni-Si2}} + (\beta + 1)C_{\text{Ni-Ni}}} V_{\text{Sub}} \quad (1)$$

where  $\beta = (C_{\text{Ni2}} + C_{\text{Ni-Si2}})/(C_{\text{Ni1}} + C_{\text{Ni-Si1}})$ .

The capacitive attractive force created from this potential difference is<sup>35</sup>

$$F_e = \left[ \frac{\delta V}{r + (r + \delta r)} \right]^2 \frac{1}{(d - 2x)^2} \quad (2)$$

where  $x$  is the displacement of nanowire tips (Figure 1b). This is the attraction force that makes nanowires lean toward each other. The vertical nanowire can be modeled as a cylindrical cantilever,<sup>34</sup> and the magnitude of this restoring force is proportional to the displacement  $x$ :

$$F_m = \frac{3EI}{L^3}x = \frac{3\pi Er^4}{4L^3}x \quad (3)$$

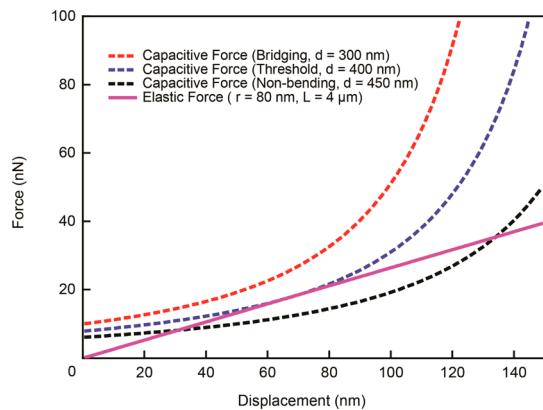


**Figure 2.** Simulation of the competition between capacitive force (dashed curves) and elastic force (purple solid curve) for bending (red), threshold (blue), and non-bending (black) situations. The horizontal axis is the lateral displacement  $x$  of the nanowire tip. The parameters used in the simulation are  $r = 80 \text{ nm}$ ,  $\delta r = 10 \text{ nm}$ ,  $L = 4 \mu\text{m}$ ,  $V_{\text{sub}} = 150 \text{ mV}$ .

where  $E = 175 \text{ GPa}$  is the elastic modulus of SiNWs<sup>36</sup> and  $I = (1/4)\pi r^4$  is the area moment of inertia for cylindrical nanowires.

The nanowire pairs will begin to bend due to attraction, but whether they can bend all the way toward each other and bridge together (creating a stiction) is determined by the competition between the capacitive attractive force and the repulsive elastic force, both of which rely on various parameters of nanowires, such as spacing, radius, and their size difference. For instance, spacing  $d$  determines the initial capacitive force and the maximum elastic force when nanowires are permanently stuck together. The simulation in Figure 2 describes three different bending scenarios when only the spacing is varied. The other parameters used in the simulation are kept the same, consistent with an actual sample fabricated for this study ( $r = 80 \text{ nm}$ ,  $L = 4 \mu\text{m}$ , and  $\delta r = 10 \text{ nm}$ ). In order for a nanowire to bridge or get in contact with one another, the capacitive force must overcome the elastic force at all times ( $F_e > F_m$  for all  $x < d$ ), which requires the initial spacing to be sufficiently small ( $d = 300 \text{ nm}$ , red curve). However, as the spacing increases to the threshold value ( $d = 400 \text{ nm}$ , blue curve),  $F_e$  and  $F_m$  will only intersect on a tangent at one particular displacement  $x_0$  (generally  $x_0 = d/3$ ). At this threshold, a small fluctuation in spacing or radius may result in different outcomes. Lastly, when the spacing goes wider than the threshold ( $d = 450 \text{ nm}$ , black curve), the capacitive force is always less than the elastic force, and spontaneous bending will not be favorable.

Besides spacing, the significance of other parameters can also be obtained from the equations for  $F_e$  and  $F_m$ . Radius  $r$  affects not only various capacitances but also the mechanical stiffness of a nanowire; furthermore, radius difference  $\delta r$  and substrate voltage  $V_{\text{sub}}$  determine the potential difference and thus the magnitude of the attractive force  $F_e$  (Supporting

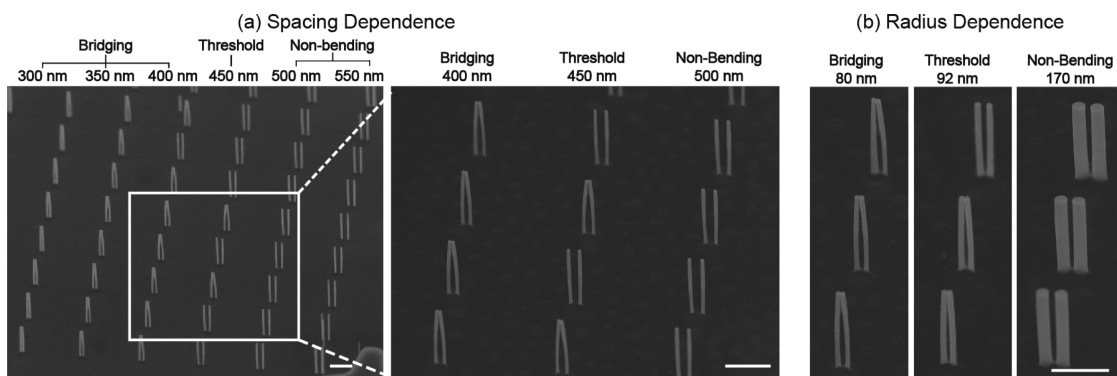


**Figure 3.** SEM images with a  $30^\circ$  tilt angle, showing various parameter dependences of nanowire spontaneous attraction. All scale bars are  $2 \mu\text{m}$ . (a) Spacing dependence. From left to right, the center-to-center spacing between a pair of nanowires increases from 300 to 550 nm, with 50 nm increments in each column. All nanowires have a radius of 160 nm and a length of  $4 \mu\text{m}$ . (b) Radius dependence. All nanowires have the same spacing of 350 nm and the same length of  $4 \mu\text{m}$ . The nanowire radii are 80, 92, and 170 nm.

Information, Figures S4 and S5). In order to further explore the significance of each parameter and find their experimental threshold value for nanowire bending, a series of controlled experiments are completed and the results are discussed in the following section.

## RESULTS AND DISCUSSION

We first evaluated the spacing dependence of spontaneous nanowire attraction. In the SEM images in Figure 3a, all nanowires are fabricated with a length of  $4 \mu\text{m}$  and a radius of 80 nm, with a radius standard deviation of  $\pm 8.7 \text{ nm}$ . From left to right, the spacing between nanowire pairs increases from 300 to 550 nm with an increment of 50 nm for each column. We found that all the nanowires with spacing  $d \leq 350 \text{ nm}$  are bent and stuck in pairs, forming a nanowire bridge structure. Some nanowires at  $d = 400\text{--}450 \text{ nm}$  appear separated, while they all become completely separated or nonbending at  $d \geq 500 \text{ nm}$ . To quantify our observations, a column with more than 80% of bridging nanowire pairs is defined as a “bridging column”. Likewise, a “threshold column” means there are 20–80% bridging nanowires, and a “nonbending column” has most NW pairs separated (more than 80%). The threshold value in this particular test is found between  $d = 400$  and  $450 \text{ nm}$ , which is very close to the theoretical threshold of  $d = 400 \text{ nm}$  with our model (Figure 2). It is clear that the spontaneous bending favors smaller spacing because the capacitive attractive force drops quadratically over distance.

Notice that once the nanowires bend and form a bridge, the junction will not be easily broken due to the strong attraction caused by dispersion forces (van der Waals force/Casimir force) at extremely small distance. However, the long-range attraction that brings nanowires together is dominated by the capacitive force because the magnitude of these short-ranged forces is negligible compared with the elastic force at initial nanowire spacing of several hundreds of nanometers (for details, see Supporting Information, Figures S1 and S2).

The second set of experiments examines the effect of a different radius on nanowire spontaneous bending. Spacing and length of nanowires are fixed at 350 nm and  $4 \mu\text{m}$ , respectively (Figure 3b), while the radius varies from 80 to 170 nm. We define radius as measured across the center of the nanowires since our simulation (see Supporting Information, Figure S6) has shown that, even in the case of nonuniform nanowire diameters or tapered wires, the threshold calculated for electrostatic bending is well approximated with a uniform wire with the center or average radius. The threshold value for the radius is found at 92 nm, where nonbending nanowires begin to show up. In our model, radius  $r$  plays a significant role in determining not only the capacitances on a nanowire but also its mechanical stiffness. Both capacitive and elastic forces show very strong dependence on radius in eqs 2 and 3. Notably, in Figure 3b, a small change of average radius of 12 nm is enough to bring a completely different result for bridging or nonbending.

To summarize these experiments, we plot in Figure 4 all experimental data points collected, categorized into three groups: red hollow circles, blue solid triangles, and black hollow squares represent nanowire pairs in the bridging columns, threshold columns, and nonbending columns, respectively. Similar to Figure 2, for each combination of spacing/radius, we can calculate and determine from our model of the balance between  $F_e$  and  $F_m$  whether the nanowire pair will be in a bridging/threshold/nonbending category. In particular, for the threshold condition, Figure 4 plots a combination of spacing/diameter values (purple curve). This calculated threshold curve describes the boundary between bridging and nonbending configurations. In this simulation,  $\delta r = 8.7 \text{ nm}$  is used because it is the experimental average from the dependence tests. Note that there is only one fitting parameter in our model, which is the substrate voltage  $V_{\text{sub}}$ . By adjusting this parameter, we can fit the observed threshold column data points (blue triangle) with the theoretical boundary when  $V_{\text{sub}} = 150 \text{ mV}$ ,

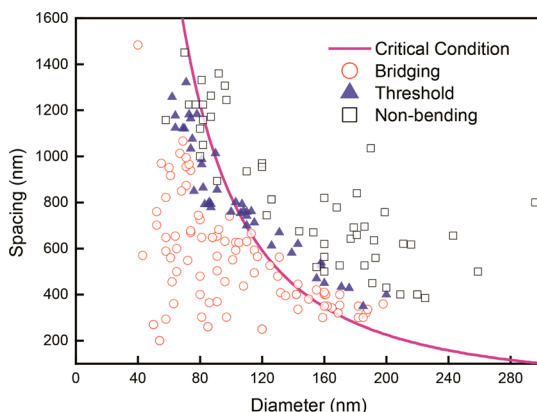


**Figure 4.** Experimental data compared with a simulation of the NW bridging critical condition. Critical curve calculated from the capacitive force model is shown as the purple curve. Data points for nanowires in bridging, threshold, or nonbending columns are represented by red hollow circles, blue solid triangles, and black hollow squares, respectively. The parameters used are  $\delta r = 8.7 \text{ nm}$ ,  $L = 4 \mu\text{m}$ ; according to experimental conditions,  $V_{\text{sub}} = 150 \text{ mV}$ .

which is consistent with the natural surface potential measured from Kelvin probe microscopy literature<sup>31</sup> for our n-type silicon substrate ( $N_d = 5 \times 10^{18} \text{ cm}^{-3}$ ).

One key consideration in our model for spontaneous adhesion or stiction due to capacitive electrostatic attractions is the inevitable size variations between nanostructures. We can test the hypothesis using pairs of nanowires with fixed radius and spacing, but with varying degrees of radius difference  $\delta r$ . If  $\delta r$  is 0, there will be zero capacitive force and no bending will occur. A threshold minimum  $\delta r$  can be calculated from the equations above. Nanowire bridging would be favored if the actual experimental radius difference exceeds that  $\delta r$ . A pair with very small  $\delta r$  will have much smaller attractive forces and will not bridge, whereas a pair with the same dimensions but a larger variation  $\delta r$  will bridge instead. The threshold  $\delta r$  can be easily calculated from our model. We carefully evaluated experimental radius differences for nanowire pairs near threshold columns from all samples and compared them with their individually calculated threshold in Figure 5. The data from experimentally bridging nanowires are shown with red dots, and the nonbending ones are shown with black squares. Notably, most bridging nanowires (84.3% of 32 bridging pairs) indeed have a size difference larger than the threshold, and the majority of nonbending nanowires (94.3% of 35 nonbending pairs) also follows the model because their size difference is smaller than the threshold. The consistency between the experimental data and the model prediction in both Figure 4 and Figure 5 strongly suggests that the principle mechanism for spontaneous attraction is the capacitive force induced by size variations in nanostructures.

Additional experiments on size difference dependence are also done with intentionally fabricated

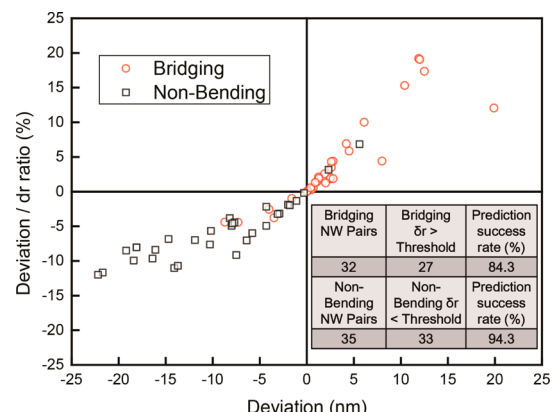


**Figure 5.** Study of the radius difference dependence with comparison between experimental data and simulation results.  $\delta r$  is the experimental value of the radius difference between each pair of nanowires. The deviation of the experimental  $\delta r$  from the calculated threshold  $\delta r$  is shown on the horizontal axis; the ratio between deviation and experimental  $\delta r$  is shown on the vertical axis. Theoretically, positive deviation ( $\delta r > \text{threshold}$ ) leads to bridging and negative deviation ( $\delta r < \text{threshold}$ ) leads to nonbending. The actual bending status for each experimental data point is indicated by different colors: red dot for bridging nanowires and black squares for nonbending nanowires. Inset table shows a summary of the number of samples and statistical percentage that follow theoretical description.

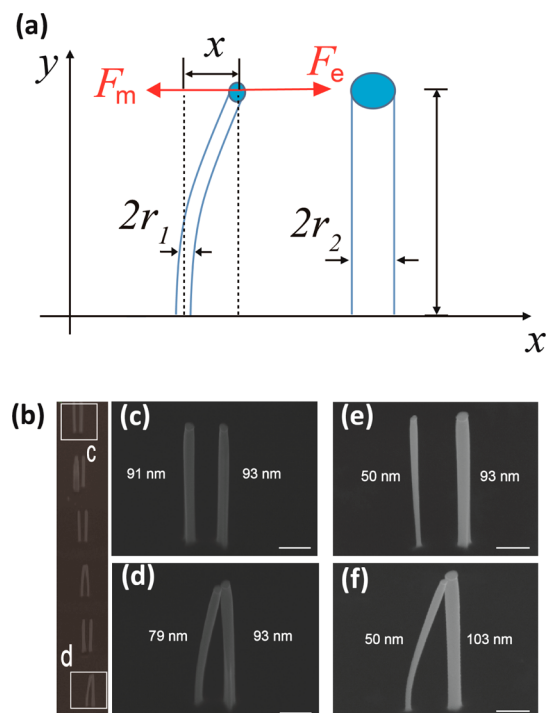


**Figure 6.** Asymmetrical nanowire bending/bridging of nanowires with a different radius. (a) Schematics for nanowire attraction and asymmetrical bending. SEM images of asymmetrical SiNW pair bending/bridging. (b-d) SEM image showing the nanowires with same spacing of 560 nm and length of  $3.4 \mu\text{m}$  in a "threshold column". Bending is favored for larger radius difference. (e,f) Two pairs of nanowires with larger size difference and same spacing of  $660 \text{ nm}$  and length of  $3.5 \mu\text{m}$ . The different radii are clearly marked on the images. All SEM images are at  $30^\circ$  tilted angle. All scale bars are 500 nm.

asymmetrical nanowire pairs (Figure 6). Our model states that the attraction between nanowires originates from capacitance difference caused by their size variance. Therefore, a larger size difference should produce a greater capacitive force that favors spontaneous bending. In contrast, nanowires with similar sizes lack the required attraction force to bend and should remain vertical. This prediction is confirmed experimentally as shown in Figure 6b–e. On the one hand, a controlled experiment in Figure 6e,f compares two nanowire pairs carefully designed and fabricated with the same spacing  $d = 660$  nm, same length  $L = 3.5\ \mu\text{m}$ , but different ratios of radii ( $r_1/r_2$ ). The radius of the thinner nanowires is strictly controlled at the same 50 nm to ensure the same mechanical properties (elastic force), whereas the thicker nanowires are 93–103 nm in radius, giving the ratio of radii of 1.96 and 2.06 for each nanowire pair correspondingly. It can be seen that a larger size difference indeed favors nanowire bridging/bending, which is consistent with the prediction of our model.

The variation of the attractive force  $F_e$  based on  $\delta r$  also explains why in the threshold column some nanowire pairs are beginning to bridge while the others remain nonbending. A careful inspection on the nanowires from a “threshold column” (Figure 6b) indicate that here the nonbending nanowire pairs have smaller radius difference (2 nm, Figure 6c) than the bridging ones (24 nm, Figure 6d), despite having the same spacing  $d = 560$  nm, length  $L = 3.4\ \mu\text{m}$ , and intended radius of 93 nm. This difference in  $\delta r$  likely comes from size variances in the patterned Ni dot mask sizes during e-beam lithography runs. Therefore, the

threshold column best illustrates how fabrication variations, under certain conditions, may lead to dramatically different fates in terms of spontaneous adhesion that ultimately may give rise to detrimental results.

## CONCLUSION

We propose and experimentally demonstrate a universal mechanism for spontaneous attraction between vertically aligned Si nanowires in terms of electrostatic interaction caused by capacitance differences due to fabrication size variations. Si nanowire pairs with varied diameter, spacing, and radius variance were fabricated using e-beam lithography and the RIE process, from which the quantitative investigation of the critical conditions for nanowire bending was performed. Small substrate charges in the capacitive network may create a bias and capacitive attraction force strong enough to overcome the inherent mechanical restoring force and cause stiction between opposing nanostructures with size variations as small as 12 nm. The capacitive force model provides guidelines for fabricating self-bridging nanowire arrays for potential applications as a nanowire bridge biological sensor or bias-controlled vertical nanomechanical switch. More broadly speaking, since capacitive force is universal in most nanostructures, this model is applicable to many other nanostructures from bottom-up assembled nanowires,<sup>2,3,37</sup> nanorods,<sup>7,17,38</sup> CNTs,<sup>9,39,40</sup> graphene<sup>10,41</sup> to top-down fabricated NEM devices.<sup>1,12–15,41</sup> These results illustrate the importance of nanofabrication precision and accuracy, which can be the determining element for the success of scientific research or practical realization of functional devices or systems.

## METHODS

The vertically aligned silicon nanowires, in pairs, were fabricated with electron-beam lithography and reactive ion etching in order to precisely control their spacing, diameter, and diameter difference. First, n-type silicon (Ultasil corp. U-7838, N/Sb(1-1-1), resistivity 0.005–0.020 ohm\*cm, with an estimated doping concentration of  $N_d = 5 \times 10^{18}\ \text{cm}^{-3}$ ) substrates were cleaned with acetone, isopropyl alcohol (IPA), and DI water for 5 min with sonication. A 200 nm thick methyl methacrylate (MMA) layer and a 200 nm thick poly(methyl methacrylate) (PMMA) e-beam resist layer were deposited on a silicon wafer by spin-coating and baked on a hot plate at 180 °C for 90 and 120 s, respectively. Next, metal (nickel) dot arrays with various spacings and diameters were patterned on the silicon wafers by a JEOL 6400 SEM/NPGS e-beam lithography system as RIE masks to fabricate nanowires. The pattern produces a gradual variation in nanowire spacing with an increment of 50 nm between each group. Different diameters were attained with increasing dosages under 30 kV e-beam exposure. The patterned film was developed in a 3:1 mixed solution of IPA and methyl isobutyl ketone for 120 s. Afterward, a 50 nm thick nickel thin film was deposited onto the wafers by a Themoscal BJD 1800 e-beam evaporator. In the lift-off process, PMMA and MMA were removed with acetone, leaving the patterned nickel nanodots on top as metal masks for the following RIE. RIE process was done using an Oxford Plasmalab 100 RIE/ICP chamber with a mixed gas of SF<sub>6</sub> and C<sub>4</sub>F<sub>8</sub>. Vertically aligned SiNW arrays were formed after the unmasked silicon was etched away. Finally, the bending and bridging

of SiNW arrays were studied with a high-resolution scanning electron microscope (FEI SFESEM UHR SEM).

*Conflict of Interest:* The authors declare no competing financial interest.

*Acknowledgment:* J.X. acknowledges support from NSF under Award ECCS-0955199 and CBET-1336428 as well as support from the Hellman Fellowship. D.W. acknowledges the financial support for this work by the Department of Energy (DOE DE-FG36-08G018016) and the National Science Foundation (NSF ECCS0901113 and CBET1236155). D.W. also acknowledges Drs. R. Rao and B. Frühberger for their support. Z.S. acknowledges Jie Min from Prof. Peter Asbeck's group for his support and helpful discussions. The authors acknowledge UCSD NANO3 staff for their professional support.

*Supporting Information Available:* Analysis for nanowire adhesion after bridging and comparisons of capacitive forces with van de Waals and Casimir forces at different ranges. Effect of applied substrate voltage and tapering of the nanowires as well as a parametric analysis of the capacitive and elastic forces. Analysis of a generic model on an insulating substrate and without a metal cluster on the nanowire tips. This material is available free of charge via the Internet at <http://pubs.acs.org>.

## REFERENCES AND NOTES

1. Loh, O. Y.; Espinosa, H. D. Nanoelectromechanical Contact Switches. *Nat. Nanotechnol.* **2012**, 7, 283–295.

2. Lu, W.; Lieber, C. M. Nanoelectronics from the Bottom Up. *Nat. Mater.* **2007**, *6*, 841–850.
3. Li, Y.; Qian, F.; Xiang, J.; Lieber, C. M. Nanowire Electronic and Optoelectronic Devices. *Mater. Today* **2006**, *9*, 18–27.
4. Liu, J.; Lee, S.; Lee, K.; Ahn, Y. H.; Park, J. Y.; Koh, K. H. Bending and Bundling of Metal-Free Vertically Aligned ZnO Nanowires due to Electrostatic Interaction. *Nanotechnology* **2008**, *19*, 185607.
5. Khorasaninejad, M.; Abedzadeh, N.; Singh Jawanda, A.; O, N.; Anantram, M. P.; Singh Saini, S. Bunching Characteristics of Silicon Nanowire Arrays. *J. Appl. Phys.* **2012**, *111*, 044328.
6. Chen, B.; Gao, Q.; Chang, L.; Wang, Y.; Chen, Z.; Liao, X.; Tan, H. H.; Zou, J.; Ringer, S. P.; Jagadish, C. Attraction of Semiconductor Nanowires: An *In Situ* Observation. *Acta Mater.* **2013**, *61*, 7166–7172.
7. Han, X.; Wang, G.; Zhou, L.; Hou, J. G. Crystal Orientation-Ordered ZnO Nanorod Bundles on Hexagonal Heads of ZnO Microcones: Epitaxial Growth and Self-Attraction. *Chem. Commun.* **2006**, *212*–214.
8. Wang, X.; Summers, C. J.; Wang, Z. L. Self-Attraction among Aligned Au/ZnO Nanorods under Electron Beam. *Appl. Phys. Lett.* **2005**, *86*, 013111.
9. De Volder, M. F. L.; Vidaud, D. O.; Meshot, E. R.; Tawfick, S.; Hart, A. J. Self-Similar Organization of Arrays of Individual Carbon Nanotubes and Carbon Nanotube Micropillars. *Microelectron. Eng.* **2010**, *87*, 1233–1238.
10. Li, G.; Yilmaz, C.; An, X.; Somu, S.; Kar, S.; Joon Jung, Y.; Busnaina, A.; Wan, K.-T. Adhesion of Graphene Sheet on Nano-patterned Substrates with Nano-pillar Array. *J. Appl. Phys.* **2013**, *113*, 244303.
11. Ardito, R.; Corigliano, A.; Frangi, A. Modelling of Spontaneous Adhesion Phenomena in Micro-electro-mechanical Systems. *Eur. J. Mech., A: Solids* **2013**, *39*, 144–152.
12. Zaghloul, U.; Bhushan, B.; Pons, P.; Papaioannou, G. J.; Coccetti, F.; Plana, R. Nanoscale Characterization of Different Stiction Mechanisms in Electrostatically Driven MEMS Devices Based on Adhesion and Friction Measurements. *J. Colloid Interface Sci.* **2011**, *358*, 1–13.
13. Wagner, T. J.; Vella, D. Switch on, Switch off: Stiction in Nanoelectromechanical Switches. *Nanotechnology* **2013**, *24*, 275501.
14. Zaghloul, U.; Papaioannou, G.; Bhushan, B.; Coccetti, F.; Pons, P.; Plana, R. On the Reliability of Electrostatic NEMS/ MEMS Devices: Review of Present Knowledge on the Dielectric Charging and Stiction Failure Mechanisms and Novel Characterization Methodologies. *Microelectron. Reliab.* **2011**, *51*, 1810–1818.
15. Lee, J. O.; Song, Y. H.; Kim, M. W.; Kang, M. H.; Oh, J. S.; Yang, H. H.; Yoon, J. B. A Sub-1-Volt Nanoelectromechanical Switching Device. *Nat. Nanotechnol.* **2013**, *8*, 36–40.
16. Patton, S. T.; Zabinski, J. S. Failure Mechanisms of Capacitive MEMS RF Switch Contacts. *Tribol. Lett.* **2005**, *19*, 265–272.
17. Lu, X.; Zheng, D.; Zhai, T.; Liu, Z.; Huang, Y.; Xie, S.; Tong, Y. Facile Synthesis of Large-Area Manganese Oxide Nanorod Arrays as a High-Performance Electrochemical Supercapacitor. *Energy Environ. Sci.* **2011**, *4*, 2915–2921.
18. Hu, L.; Chen, G. Analysis of Optical Absorption in Silicon Nanowire Arrays for Photovoltaic Applications. *Nano Lett.* **2007**, *7*, 3249–3252.
19. Abadyan, M. R.; Beni, Y. T.; Noghrehabadi, A. Investigation of Elastic Boundary Condition on the Pull-in Instability of Beam-Type NEMS under van der Waals Attraction. *Procedia Eng.* **2011**, *10*, 1724–1729.
20. Chen, C.; Li, S.; Dai, L.; Qian, C. Buckling and Stability Analysis of a Piezoelectric Viscoelastic Nanobeam Subjected to van der Waals Forces. *Commun. Nonlinear Sci. Numer. Simul.* **2014**, *19*, 1626–1637.
21. Rodriguez, A. W.; Capasso, F.; Johnson, S. G. The Casimir Effect in Microstructured Geometries. *Nat. Photonics* **2011**, *5*, 211–221.
22. Agache, V.; Quévy, E.; Collard, D.; Buchaillot, L. Stiction-Controlled Locking System for Three-Dimensional Self-Assembled Microstructures: Theory and Experimental Validation. *Appl. Phys. Lett.* **2001**, *79*, 3869.
23. Chandra, D.; Yang, S. Capillary-Force-Induced Clustering of Micropillar Arrays: Is It Caused by Isolated Capillary Bridges or by the Lateral Capillary Meniscus Interaction Force? *Langmuir* **2009**, *25*, 10430–10434.
24. Duprat, C.; Protiere, S.; Beebe, A. Y.; Stone, H. A. Wetting of Flexible Fibre Arrays. *Nature* **2012**, *482*, 510–513.
25. Hill, J. J.; Haller, K.; Gelfand, B.; Ziegler, K. J. Eliminating Capillary Coalescence of Nanowire Arrays with Applied Electric Fields. *ACS Appl. Mater. Interfaces* **2010**, *2*, 1992–1998.
26. Tang, Y.; Zhao, D.; Chen, J.; Wanderka, N.; Shen, D.; Fang, F.; Guo, Z.; Zhang, J.; Wang, X. Capillary-Driven Assembly of ZnO Nanowire Arrays into Micropatterns. *Mater. Chem. Phys.* **2010**, *121*, 541–548.
27. Liu, J.-L.; Xia, R.; Zhou, Y.-T. Stiction of a Nano-beam with Surface Effect. *Chin. Phys. Lett.* **2011**, *28*, 116201.
28. Pokroy, B.; Kang, S. H.; Mahadevan, L.; Aizenberg, J. Self-Organization of a Mesoscale Bristle into Ordered, Hierarchical Helical Assemblies. *Science* **2009**, *323*, 237–240.
29. Blinov, L. M.; Sonin, A. A. Anisotropy and Effective Range of the van der Waals Forces of the Solid Crystalline Substrates Investigated by Means of Liquid Crystals. *Langmuir* **1987**, *3*, 660–661.
30. Kong, X. Y.; Ding, Y.; Yang, R.; Wang, Z. L. Single-Crystal Nanorings Formed by Epitaxial Self-Coiling of Polar Nano-belts. *Science* **2004**, *303*, 1348–1351.
31. Henning, A. K.; Hochwitz, T.; Slinkman, J.; Never, J.; Hoffmann, S.; Kaszuba, P.; Daghlian, C. Two-Dimensional Surface Dopant Profiling in Silicon Using Scanning Kelvin Probe Microscopy. *J. Appl. Phys.* **1995**, *77*, 1888–1896.
32. Breitenstein, O.; Gupta, R.; Schneider, J. Surface Potential Mapping on Crystalline Silicon on Glass Solar Modules. *J. Appl. Phys.* **2007**, *102*, 024511.
33. Doukkali, A.; Ledaïn, S.; Guasch, C.; Bonnet, J. Surface Potential Mapping of Biased pn Junction with Kelvin Probe Force Microscopy: Application to Cross-Section Devices. *Appl. Surf. Sci.* **2004**, *235*, 507–512.
34. Mizsei, J. Silicon Surface Passivation by Static Charge. *Appl. Surf. Sci.* **2006**, *252*, 7691–7699.
35. Lekner, J. Electrostatic Force between Two Conducting Spheres at Constant Potential Difference. *J. Appl. Phys.* **2012**, *111*, 076102.
36. Song, J.; Wang, X.; Riedo, E.; Wang, Z. L. Elastic Property of Vertically Aligned Nanowires. *Nano Lett.* **2005**, *5*, 1954–1958.
37. Takahashi, T.; Takei, K.; Adabi, E.; Fan, Z.; Niknejad, A. M.; Javey, A. Parallel Array InAs Nanowire Transistors for Mechanically Bendable, Ultrahigh Frequency Electronics. *ACS Nano* **2010**, *4*, 5855–5860.
38. Pacholski, C.; Kornowski, A.; Weller, H. Self-Assembly of ZnO: From Nanodots to Nanorods. *Angew. Chem., Int. Ed.* **2002**, *41*, 1188–1191.
39. Baughman, R. H.; Zakhidov, A. A.; de Heer, W. A. Carbon Nanotubes—The Route toward Applications. *Science* **2002**, *297*, 787–792.
40. Li, J.; Papadopoulos, C.; Xu, J. M.; Moskovits, M. Highly-Ordered Carbon Nanotube Arrays for Electronics Applications. *Appl. Phys. Lett.* **1999**, *75*, 367–369.
41. Bunch, J. S.; van der Zande, A. M.; Verbridge, S. S.; Frank, I. W.; Tanenbaum, D. M.; Parpia, J. M.; Craighead, H. G.; McEuen, P. L. Electromechanical Resonators from Graphene Sheets. *Science* **2007**, *315*, 490–493.